Article ID: 1000-324X(2015)05-0549-06 **DOI:** 10.15541/jim20140574

Synthesis and Enhanced Photocatalytic Activity of Er^{3+}-doped $ZnWO_4$

ZHOU Yu, ZHANG Zhi-Jie, XU Jia-Yue, CHU Yao-Qing, YOU Ming-Jiang

(Institute of Crystal Growth, School of Materials Science and Engineering, Shanghai Institute of Technology, Shanghai 201418, China)

Abstract: Er^{3+}-doped $ZnWO_4$ nanorods with different doping concentrations were synthesized by a hydrothermal method. The as-prepared products were characterized by XRD, TEM and DRS. The photocatalytic activities of the as-prepared $ZnWO_4$ samples were evaluated by photo-degradation of RhB under simulated solar light irradiation and the effects of Er^{3+} doping on the photocatalytic activity of $ZnWO_4$ were investigated. The result showed that the sample with the doping concentration of 2mol% exhibited the best photocatalytic performance, which could be ascribed to the promoted charge separation efficiency of Er^{3+}-doped $ZnWO_4$.

Key words: Er^{3+}-doped $ZnWO_4$; photocatalyst; Rhodamine B; charge separation

Water pollution is one of the most serious environmental problems in modern society. Semiconductor-mediated photocatalytic degradation is a promising technique for wastewater treatment. In recent years, semiconductor-based photocatalysis has attracted more and more attention for solving environment problems, especially for the removal of organic contaminants under sunlight[1−8].

Tungstates are widely used functional materials, and it has been confirmed that tungstates are a class of promising photocatalysts[9-11]. $ZnWO_4$ as an important member of tungstates, due to its photocatalytic properties and potential applications, has received intense research attention[12-13]. Up to now, $ZnWO_4$ has been used for water splitting and decomposition of organic pollutants under UV irradiation[14-17]. However, improvement of photocatalytic activity of $ZnWO_4$ is still indispensable because the photo-activity of $ZnWO_4$ is not high enough for the requirements of practical application.

It is known that the photocatalytic activity depends strongly on the separation efficiency of photo-generated electron-hole pairs. Up to date, great efforts have been made to facilitate the electron-hole separation and enhance the photocatalytic activity of $ZnWO_4$, including cation doping[18-19], anion doping such as fluorine or chlorine[12, 20-21], and coupling with other semiconductors such as Bi_2WO_6[22] or ZnO[23]. Especially, doping of lanthanide ions with 4f electron configuration has been proposed as an effective way to eliminate the recombination of electron-hole pairs. For example, it has been reported that doping with Eu^{3+}, Er^{3+} or Ce^{4+} could improve the photocatalytic activity of TiO_2[24-25], and doping with Er^{3+} could enhance the photocatalytic activity of Bi_2WO_6[26]. Inspired by those progresses, we intended to design a doped $ZnWO_4$ photocatalyst by introducing lanthanide ion Er^{3+}. To the best of our knowledge, there are no reports on the photocatalytic activity of Er^{3+}-doped $ZnWO_4$.

In this work, Er^{3+}-doped $ZnWO_4$ photocatalysts were synthesized by a simple hydrothermal process. The product synthesized by this method had uniform phase and good crystallization. Moreover, the shape and size of the product could be controlled. The photo-activity evaluation, *via* the degradation of RhB under simulated solar light, demonstrated that doping appropriate amount of Er^{3+} could enhance the photocatalytic performance of $ZnWO_4$ effectively. Moreover, the mechanism of the photocatalytic process for Er^{3+}-doped $ZnWO_4$ was discussed in detail.

1 Experimental procedures

1.1 Synthesis

All chemicals used were analytic grade reagents without further purification. The experimental process of synthesizing Er^{3+}-doped $ZnWO_4$ photocatalysts was as follows: 1 mmol of $Na_2WO_4{\cdot}2H_2O$ was dissolved in 10 mL of deionized water to obtain solution A. Meanwhile, 1 mmol of $Zn(NO_3)_2{\cdot}6H_2O$ was dissolved in

Received date: 2014-11-11; **Modified date:** 2014-12-29; **Published online:** 2015-02-16
Foundation item: National Natural Science Foundation of China (51342007, 51402194); Shanghai Science and Technology Committee (11JC1412400, 14YF1410700)
Biography: ZHOU Yu(1989–), male, candidate of master degree. E-mail: zhouyu564022786@163.com
Corresponding author: ZHANG Zhi-Jie, PhD. E-mail: zjzhang@sit.edu.cn; XU Jia-Yue, Professor. E-mail: xujiayue@sit.edu.cn

10 mL of deionized water to obtain solution B. Then an appropriate amount of $Er(NO_3)_3$ solution was slowly added to solution A under stirring. After that, solution B was added to the mixed solution to obtain a white suspension. The pH value of the suspension was adjusted to 8 by the addition of NaOH solution, then sealed in a Teflon-lined stainless steel autoclave and heated at 433 K for 16 h under autogenous pressure. The obtained solid product was washed thoroughly with deionized water and dried at 333 K. In this work, the doping concentrations of Er^{3+} were 0, 1mol%, 2mol%, 2.5mol%, 3.5mol%, 5mol%, and 7mol%, respectively.

1.2 Characterization

The phase and composition of as-prepared samples were measured by the powder X-ray diffractometer operated at 40 kV and 30 mA using Cu Kα radiation (λ=0.15418 nm). The morphologies of the products were obtained by transmission electron microscope (FEI tecnai G2F30). UV-Vis DRS was performed on a Cary 5000 UV-Vis spectrophotometer.

1.3 Photocatalytic test

The photocatalytic activities of the as-prepared samples were evaluated by the photocatalytic degradation of RhB under simulated solar light using a 500 W Xe lamp as the light source. The experiments were performed at room temperature as follows: 0.05 g of photocatalyst was added into 50 mL of RhB solution (1×10^{-5} mol/L). The suspensions were magnetically stirred in the dark for 0.5 h in order to ensure the adsorption/desorption equilibrium between the photocatalyst powders and the solution. 3 mL of suspensions were sampled every 0.5 h and centrifuged to remove the photocatalyst powders. Evaluation of the photocatalytic activities of the photocatalysts was conducted by recording the variations of the absorption band maximum through a UV-Vis spectrophotometer (Cary 5000) and the concentration of RhB was analyzed by recording the variations of the absorption band maximum (552 nm).

2 Results and discussion

2.1 Crystal structure

The XRD patterns of the as-prepared Er^{3+}-doped $ZnWO_4$ samples with different doping concentrations were shown in Fig. 1. All the peaks in the patterns matched well with the characteristic reflections of zinc tungstate (JCPDS 15-0774). No signals for any other phases were observed, which indicated that the products were pure phase and Zn^{2+} was successfully replaced by Er^{3+} and Er^{3+} was uniformly incorporated into the lattice.

2.2 UV-Vis spectra

Figure 2 showed the diffuse reflectance spectra (DRS) of pure $ZnWO_4$ and the 2mol% Er^{3+}-doped $ZnWO_4$ sample.

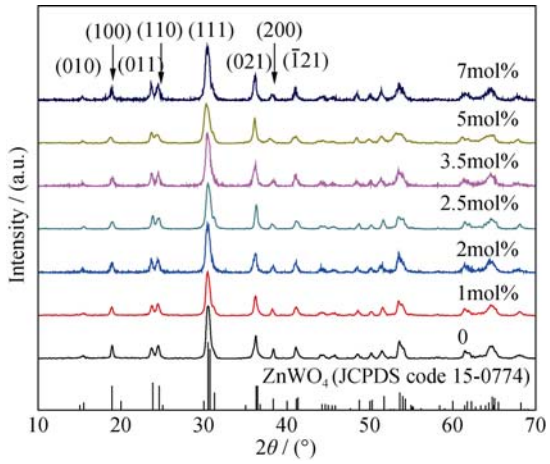

Fig. 1 Powder X-ray diffraction patterns for Er^{3+}-doped $ZnWO_4$ with different doping concentrations

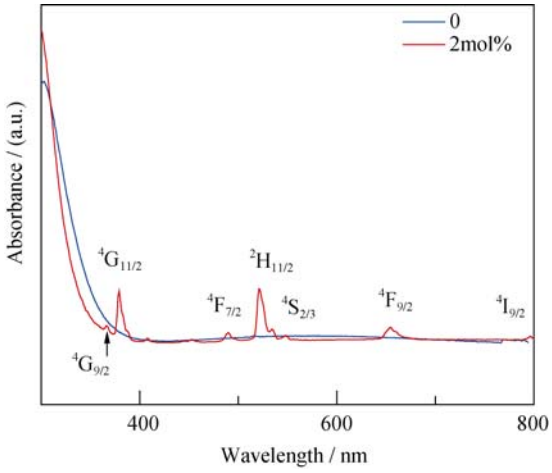

Fig. 2 UV-Vis diffuses reflectance spectra of the as-prepared $ZnWO_4$ samples

It indicated that pure $ZnWO_4$ presented an absorption edge around 400 nm. For the Er^{3+}-doped $ZnWO_4$ sample, there were also some sharp absorption bands originated from characteristic f–f or f–d transition of the Er^{3+} ion. The transition peaks, which centered at 365, 378, 489, 520, 548, 653, and 795 nm, were attributed to the transitions of $^4I_{15/2}\rightarrow{}^4G_{9/2}$, $^4I_{15/2}\rightarrow{}^4G_{11/2}$, $^4I_{15/2}\rightarrow{}^4F_{7/2}$, $^4I_{15/2}\rightarrow{}^4H_{11/2}$, $^4I_{15/2}\rightarrow{}^4S_{3/2}$, $^4I_{15/2}\rightarrow{}^4F_{9/2}$, $^4I_{15/2}\rightarrow{}^4I_{9/2}$, respectively[27].

2.3 Morphology

The morphologies and microstructures of pure $ZnWO_4$ and the 2mol% Er^{3+}-doped $ZnWO_4$ samples were investigated with TEM, as shown in Fig. 3. It could be seen clearly that the as-prepared samples exhibited nanorods structure, which indicated that Er^{3+} doping did not change the morphologies of $ZnWO_4$. Moreover, pure $ZnWO_4$ nanorods were 35 nm in diameter and 40–60 nm in length (Fig. 3(a)) and the Er^{3+}-doped $ZnWO_4$ were 10 nm in diameter and 30–70 nm in length (Fig. 3(c)). This is because that doping Er^{3+} could influence the growing interface and finally change the diameter of $ZnWO_4$

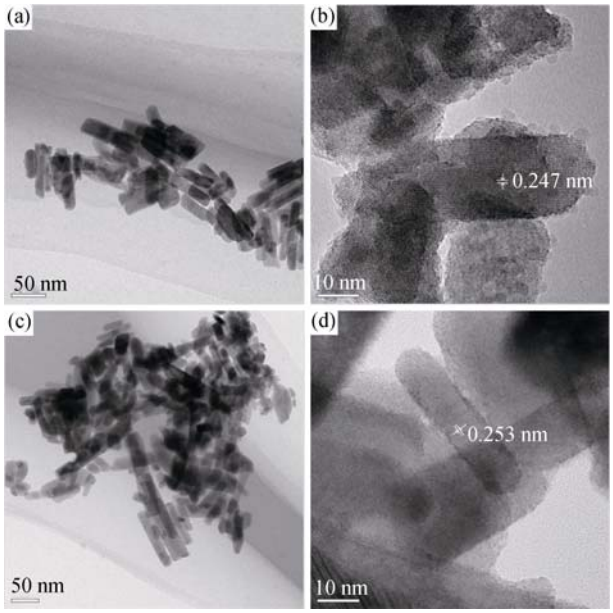

Fig. 3　Typical TEM and HRTEM images of the as-synthesized $ZnWO_4$ samples
(a, b) Pure $ZnWO_4$; (c, d) 2mol% Er^{3+}-doped $ZnWO_4$

nanorods according to the chemical bonding theory of single crystal growth[28-29]. The HRTEM images showed clear lattice fringes of d=0.247 nm for pure $ZnWO_4$ (Fig. 3(b)) and d=0.253 nm for Er^{3+}-doped $ZnWO_4$ (Fig. 3(d)), which matched the d-spacing of the (021) plane of $ZnWO_4$.

2.4　Photocatalytic activities of the catalysts

The absorption spectra of RhB after degradation by the 2mol% Er^{3+}-doped $ZnWO_4$ sample was shown in Fig. 4(a). It was clear that the absorption of RhB was negligible after 3 h, which indicated that RhB was degraded completely. The photocatalytic activities of the Er^{3+}-doped $ZnWO_4$ samples were determined by comparing the degradation efficiency of RhB under simulated solar light irradiation (Fig. 4 (b)). Blank test showed that the degradation of RhB was negligible in the absence of photocatalyst under light illumination. It could be seen that the photocatalytic activity of $ZnWO_4$ was enhanced with the introduction of Er^{3+} and reached a maximum with the doping concentration of 2mol%. Then the photocatalytic activity decreased when the doping concentration of Er^{3+} further increased.

Moreover, the comparison of the apparent rate constant k in Fig. 5 showed the 2mol% Er^{3+}-doped $ZnWO_4$ sample had the highest k value in the degradation of RhB (1.411 h^{-1}), while that of pure $ZnWO_4$ was only 0.534 h^{-1}. In other words, the photocatalytic activity of the 2mol% Er^{3+}-doped $ZnWO_4$ sample was 2.64 times that of pure $ZnWO_4$. This result indicated that Er^{3+} doping played an important role in the enhancement of the photocatalytic activity.

The photocatalytic activities of the 2mol% Er^{3+}-doped $ZnWO_4$ sample under different conditions were shown in Fig. 6. It could be seen clearly that when the pH value of the RhB solution was 3, the sample showed the highest photocatalytic activity (Fig. 6(a)). This is because the pH value can change the surface electrical property of $ZnWO_4$ and its adsorption ability. Moreover, it could be seen from Fig. 6(b) that when the amount of the photocatalyst and the concentration of RhB were not changed, the more amount of RhB solution was, the weaker the photocatalytic activity was. When the amount of RhB solution increased, fewer photons could penetrate through the solution, which led to the decreased photocatalytic activity.

2.5　Mechanism of the enhanced photo-activities

It's known that the photocatalysis efficiency is determined by the competition between the charge separation process and the charge recombination process, and a desired photocatalyst is expected to promote the charge transfer process while suppressing the recombination process. The introduction of Er^{3+} could facilitate the charge separation process in such a way: As illustrated in

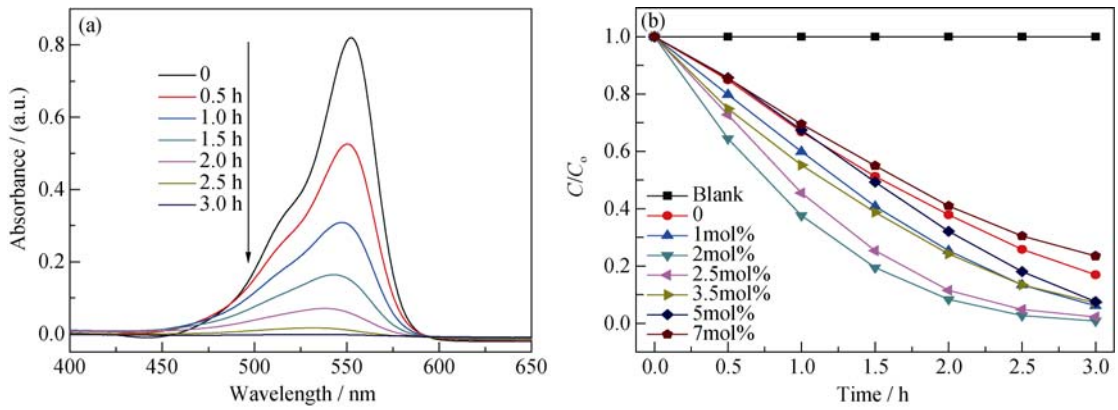

Fig. 4　The absorption spectra of RhB after degradation by the 2mol% Er^{3+}-doped $ZnWO_4$ sample (a) and degradation efficiency of RhB by the as-prepared samples under a 500 W Xe lamp as a function of time (b)

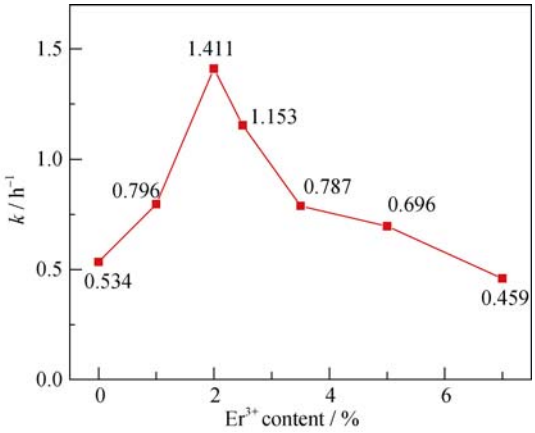

Fig. 5 The rate constant k of Er^{3+}-doped $ZnWO_4$ with different doping concentrations

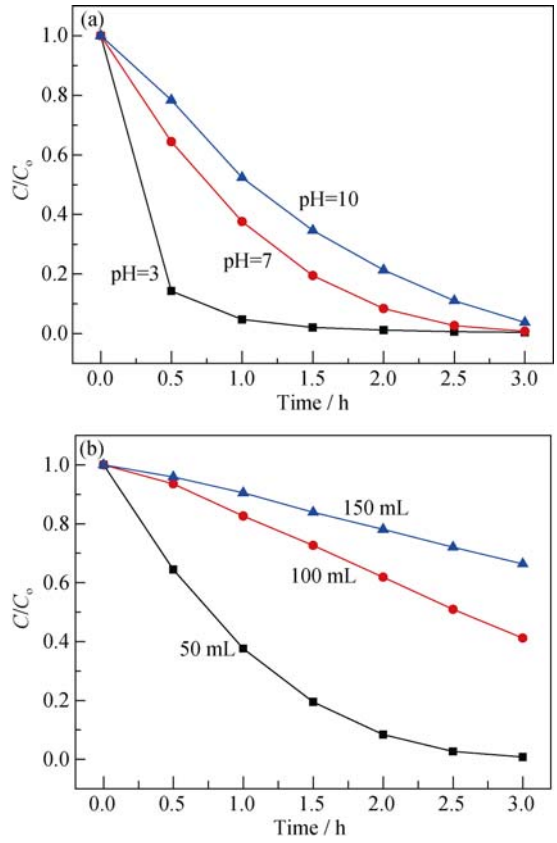

Fig. 6 Degradation efficiency of RhB by the 2mol% Er^{3+}-doped $ZnWO_4$ sample under different conditions
(a) Different pH values of the RhB solution; (b) Different amounts of the RhB solution

Fig. 7, the presence of Er^{3+} ions might cause the following steps[30-31].

$$ZnWO_4 + h\nu \rightarrow ZnWO_4(e^- + h^+) \quad (1)$$

$$Er^{3+} + e^- \rightarrow Er^{2+} \quad (2)$$

$$Er^{2+} + O_2 \rightarrow Er^{3+} + O_2^{\cdot -} \quad (3)$$

$$h^+, O_2^{\cdot -} + RhB \rightarrow \text{degraded products} \quad (4)$$

In the photocatalytic process, the Er^{3+} ion trapped the photo-generated electrons and formed a reduction species

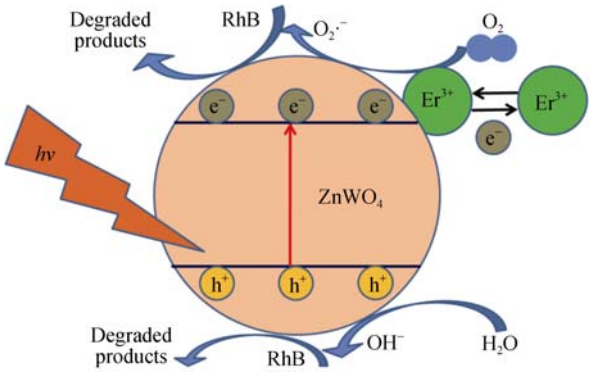

Fig. 7 Schematic for the photocatalytic mechanism of Er^{3+}-doped $ZnWO_4$

Er^{2+} ion, and then the Er^{2+} could be oxidized back to Er^{3+} by the adsorbed oxygen. The electron-hole recombination rate could be reduced due to the recycle reactions. In addition, when Er^{3+} was introduced into the system, the substitution of Er^{3+} for Zn^{2+} led to the formation of $[Er_{Zn}]^+$ defects. Meanwhile, $[V_{Zn}]^{2-}$ cation vacancies were generated for charge compensation. The $\{2[Er_{Zn}]^+ - [V_{Zn}]^{2-}\}$ defect groups could act as electron and hole traps, so as to inhibit the recombination and extend the lifetime of charge carriers. Therefore, appropriate doping amount of Er^{3+} could enhance the photocatalytic process by suppressing the charge recombination effectively. However, when the doping concentration of Er^{3+} increased further, excess of Er^{3+} could act as electron/hole recombination centers, which led to a decreased photocatalytic activity. So there existed an optimum doping concentration for Er^{3+}.

3 Conclusion

Er^{3+}-doped $ZnWO_4$ photocatalysts were synthesized by a hydrothermal method. The effects of Er^{3+} doping on the photocatalytic activity of $ZnWO_4$ catalysts were investigated. 2mol% Er^{3+}-doped $ZnWO_4$ sample exhibited the highest photocatalytic activity, which was 2.64 times that of pure $ZnWO_4$. The enhanced photocatalytic activity could be attributed to the higher charge separation efficiency brought by Er^{3+} doping. Our work indicates that the introduction of lanthanide ion could be a plausible strategy to develop efficient photocatalysts for environmental remediation and is worth to be extended to the preparation of other photocatalysts with high activity.

References:

[1] HAGFELDT A, GRAETZEL M. Light-induced redox reactions in nanocrystalline systems. *Chemical Reviews*, 1995, **95(1):** 49–68.

[2] HOFFMANN M R, MARTIN S T, CHOI W, *et al*. Environmental

applications of semiconductor photocatalysis. *Chemical Reviews*, 1995, **95(1):** 69–96.

[3] ZOU Z, YE J, SAYAMA K, *et al*. Photocatalytic and photophysical properties of a novel series of solid photocatalysts, $BiTa_{1-x}Nb_xO_4$ ($0 \leqslant x \leqslant 1$). *Chemical Physics Letters*, 2001, **343(3):** 303–308.

[4] TSUJI I, KATO H, KUDO A. Photocatalytic hydrogen evolution on ZnS-$CuInS_2$-$AgInS_2$ solid solution photocatalysts with wide visible light absorption bands. *Chemistry of Materials*, 2006, **18(7):** 1969–1975.

[5] LI G S, ZHANG D Q, YU J C. A new visible-light photocatalyst: CdS quantum dots embedded mesoporous TiO_2. *Environmental Science & Technology*, 2009, **43(18):** 7079–7085.

[6] AKYOL A, BAYRAMOGLU M. Photocatalytic performance of ZnO coated tubular reactor. *Journal of Hazardous Materials*, 2010, **180(1):** 466–473.

[7] LIU Z, BAI H, SUN D. Facile fabrication of hierarchical porous TiO_2 hollow microspheres with high photocatalytic activity for water purification. *Applied Catalysis B: Environmental*, 2011, **104(3):** 234–238.

[8] ZHANG Z, WANG W, GAO E, *et al*. Photocatalysis coupled with thermal effect Induced by SPR on Ag-loaded Bi_2WO_6 with enhanced photocatalytic activity. *Journal of Physical Chemistry C*, 2012, **116(49):** 25898–25903.

[9] TANG J, ZOU Z, YE J. Photophysical and photocatalytic properties of $AgInW_2O_8$. *Journal of Physical Chemistry B*, 2003, **107(51):** 14265–14269.

[10] FU H, ZHANG L, YAO W, *et al*. Photocatalytic properties of nanosized Bi_2WO_6 catalysts synthesized *via* a hydrothermal process. *Applied Catalysis B: Environmental*, 2006, **66(1):** 100–110.

[11] ZHANG Z, WANG W, SHANG M, *et al*. Low-temperature combustion synthesis of $B_{i2}W_{O6}$ nanoparticles as a visible-light-driven photocatalyst. *Journal of Hazardous Materials*, 2010, **177(1):** 1013–1018.

[12] HUANG G, ZHU Y. Enhanced photocatalytic activity of $ZnWO_4$ catalyst *via* fluorine doping. *Journal of Physical Chemistry C*, 2007, **111(32):** 11952–11958.

[13] GARADKAR K M, GHULE L A, SAPNAR K B, *et al*. A facile synthesis of $ZnWO_4$ nanoparticles by microwave assisted technique and its application in photocatalysis. *Materials Research Bulletin*, 2013, **48(3):** 1105–1109.

[14] VERGADOS J D. The neutrinoless double beta decay from a modern perspective. *Physics Reports*, 2002, **361(1):** 1–56.

[15] TAN G, ZHANG L, WEI S, *et al*. Microwave hydrothermal synthesis and photocatalytic properties of $ZnWO_4$ nanorods. C*rystal Research and Technology*, 2012, **47(12):** 1279–1283.

[16] HUANG G, ZHANG C, ZHU Y. $ZnWO_4$ photocatalyst with high activity for degradation of organic contaminants. *Journal of Alloys and Compounds*, 2007, **432(1):** 269–276.

[17] SHI R, WANG Y, LI D, *et al*. Synthesis of $ZnWO_4$ nanorods with [100] orientation and enhanced photocatalytic properties. *Applied Catalysis B: Environmental*, 2010, **100(1):** 173–178.

[18] DONG T, LI Z, DING Z, *et al*. Characterizations and properties of Eu^{3+}-doped $ZnWO_4$ prepared *via* a facile self-propagating combustion method. *Materials Research Bulletin*, 2008, **43(7):** 1694–1701.

[19] SU Y, ZHU B, GUAN K, *et al*. Particle size and structural control of $ZnWO_4$ nanocrystals *via* Sn^{2+} doping for tunable optical and visible photocatalytic properties. *Journal of Physical Chemistry C*, 2012, **116(34):** 18508–18517.

[20] CHEN S, SUN S, SUN H, *et al*. Experimental and theoretical studies on the enhanced photocatalytic activity of $ZnWO_4$ nanorods by fluorine doping. *Journal of Physical Chemistry C*, 2010, **114(17):** 7680–7688.

[21] HUANG G, ZHU Y. Synthesis and photoactivity enhancement of $ZnWO_4$ photocatalysts doped with chlorine. *CrystEngComm*, 2012, **14(23):** 8076–8082.

[22] HE D, WANG L, XU D, *et al*. Investigation of photocatalytic activities over Bi_2WO_6/$ZnWO_4$ composite under UV light and its photoinduced charge transfer properties. *ACS Applied Materials & Interfaces*, 2011, **3(8):** 3167–3171.

[23] HAMROUNI A, MOUSSA N, DI PAOLA A, *et al*. Characterization and photoactivity of coupled ZnO–$ZnWO_4$ catalysts prepared by a Sol–Gel method. *Applied Catalysis B: Environmental*, 2014, **154:** 379–385.

[24] YANG P, LU C, HUA N, *et al*. Titanium dioxide nanoparticles co-doped with Fe^{3+} and Eu^{3+} ions for photocatalysis. *Materials Letters*, 2002, **57(4):** 794–801.

[25] XU A W, GAO Y, LIU H Q. The preparation, characterization, and their photocatalytic activities of rare-earth-doped TiO_2 nanoparticles. *Journal of Catalysis*, 2002, **207(2):** 151–157.

[26] ZHANG Z, WANG W, YIN W, *et al*. Inducing photocatalysis by visible light beyond the absorption edge: effect of upconversion agent on the photocatalytic activity of Bi_2WO_6. *Applied Catalysis B: Environmental*, 2010, **101(1):** 68–73.

[27] YANG F, TU C, LI J, *et al*. Growth and optical property of $ZnWO_4$: Er^{3+} crystal. *Journal of Luminescence*, 2007, **126(2):** 623–628.

[28] SUN C, XUE D. Crystal growth and design of sapphire: both experimental and calculation studies of anisotropic crystal growth upon pulling directions. *Crystal Growth & Design*, 2014, **14:**

2282–2287.

[29] SUN C, XUE D. Chemical bonding theory of single crystal growth and its application to $\phi 3''$ YAG bulk crystal. *CrystEngComm*, 2014, **16(11):** 2129–2135.

[30] TSUNODA Y, SUGIMOTO W, SUGAHARA Y. Intercalation behavior of n-alkylamines into a protonated form of a layered perovskite derived from aurivillius phase $Bi_2SrTa_2O_9$. *Chemistry of materials*, 2003, **15(3):** 632–635.

[31] TIAN Y, ZHANG L, ZHANG J. A superior visible light-driven photocatalyst: europium-doped bismuth tungstate hierarchical microspheres. *Journal of Alloys and Compounds*, 2012, **537:** 24–28.

Er^{3+}掺杂 $ZnWO_4$ 的合成及光催化活性研究

周 宇, 张志洁, 徐家跃, 储耀卿, 尤明江

(上海应用技术学院 材料科学与工程学院, 晶体生长研究所, 上海 201418)

摘 要: 通过水热法合成了不同浓度 Er^{3+}掺杂 $ZnWO_4$ 纳米棒, 并通过 XRD、TEM 和 DRS 等对其进行了表征。通过在模拟太阳光照射下光降解 RhB 的速度来检测 $ZnWO_4$ 样品的光催化活性, 研究了 Er^{3+}掺杂浓度对 $ZnWO_4$ 催化活性的影响。实验结果表明, 当 Er^{3+}掺杂浓度为 2mol%时, 其光催化性能最好, 因为引进 Er^{3+}后, Er^{3+}加快了电荷分离效率。

关 键 词: Er^{3+}掺杂钨酸锌; 光催化剂; 罗丹明 B; 电荷分离

中图分类号: TQ174 **文献标识码:** A